Measurement of the 1s Lamb shift in hydrogenlike nickel

H. F. Beyer
Gesellschaft für Schwerionenforschung Darmstadt m.b.H., Postfach 11 05 52, 6100 Darmstadt, Federal Republic of Germany

P. Indelicato
National Institute of Standards and Technology, Gaithersburg, Maryland 20899

K. D. Finlayson and D. Liesen
Gesellschaft für Schwerionenforschung Darmstadt m.b.H., Postfach 11 05 52, 6100 Darmstadt, Federal Republic of Germany

R. D. Deslattes
National Institute of Standards and Technology, Gaithersburg, Maryland 20899
(Received 10 April 1990)

The wavelength of the $2p_{3/2} \rightarrow 1s_{1/2}$ transition in hydrogenlike Ni^{27+} has been measured with an accuracy of 13 ppm. Bare Ni^{28+} ions of 11.4 MeV/amu as emerging from a carbon stripper foil were decelerated to 8.4, 6.7, 5.2, and 3.1 MeV/amu and dressed in a thin target gas by electron capture. The x rays were measured with a crystal spectrometer in Johann geometry employing a position-sensitive x-ray detector. The 1s Lamb shift in hydrogenlike nickel has been found to be 5.07 ± 0.10 eV in good agreement with theory.

I. INTRODUCTION

In the past several years, measurement of radiative corrections in highly charged heavy ions has attracted increasing interest. The 1s Lamb shift, which is the largest quantum electrodynamics (QED) correction, has been measured in hydrogen by Doppler-free two-photon spectroscopy.[1,2] In more recent work,[2] the 1s Lamb shift emerges with an uncertainty of 86 ppm. It has been measured in hydrogenlike iron[3] and krypton[4] using beam-foil spectroscopy, in chlorine in a Tokamak,[5] and in argon recoil ions.[6] A measurement has also been performed starting with decelerated bare chlorine ions.[7] Resulting values for the Lamb shift are associated with uncertainties of 1.4% in argon and 4.2% in krypton.

Measurements of $2l \rightarrow 1s$ transition energies in high-Z one-electron ions provide an important test of calculations involving QED effects. Whereas higher-order contributions to the Lamb shift are hardly discernible at low Z, they dramatically increase at high Z. For nickel, the higher-order contributions already account for more than one-third of the total Lamb shift.

In this paper we report on an experiment using decelerated bare nickel ions that yields a value for the 1s Lamb shift with an estimated uncertainty of 2%. The precision of previous experiments using beam-foil or recoil-ion sources was limited by spectator-electron contamination and/or Doppler effects. For both effects it is very difficult to estimate the experimental error. Here, we report on an experiment that conceptually overcomes both difficulties. The spectator-electron problem is avoided by making use of a prevailing one-electron transfer in a thin target gas, while the Doppler effect is brought under control by measuring the x-ray spectra at four different ion-beam velocities.

II. EXPERIMENTAL METHOD

The experimental configuration used in the present work is sketched in Fig. 1. Nickel ions are accelerated in the universal linear accelerator (UNILAC) up to a specific energy of 11.4 MeV/amu and are then stripped in a 650-(μg/cm^2)-thick carbon foil giving a naked Ni^{28+} fraction of about 10%. The single-resonator structures at the end of the UNILAC are used to decelerate the beam down to final specific energies, which, for the bare ions, are 8.4, 6.7, 5.2, and 3.1 MeV/amu. The Ni^{28+} component is magnetically selected and directed to a long straight experimental section. There, a 15-m-long time-of-flight measuring device[8] allows a measurement of the ion-beam velocity with a precision of $\Delta\beta/\beta \lesssim 5 \times 10^{-4}$. The ion beam, collimated to a divergence of less than 0.7 mrad, passes through a differentially pumped gas cell containing the argon target gas at a pressure of about 0.2 mbar. The ion current ranges from 150 to 600 particle nA. The 2p states of interest in hydrogenlike Ni^{27+} are populated by one-electron capture, mainly into higher-n states followed by cascade transitions.

The x rays of about 8 keV energy are diffracted in second order by a Ge(220) crystal bent cylindrically to a radius of 976 mm. The corresponding Bragg angles are close to 50°. The center of the gas cell is located 314 mm inside the Rowland circle, which is oriented perpendicular to the ion-beam direction. We use a two-dimensional position-sensitive proportional counter (PSD) having a multiwire anode and backgammon cathode structure of the general type previously reported,[9] but incorporating several recent improvements.[10] The anode wires of this detector, which are separated by 2.032 mm, are oriented along the direction of dispersion (x direction). By charge division of the two cathode signals, a position resolution

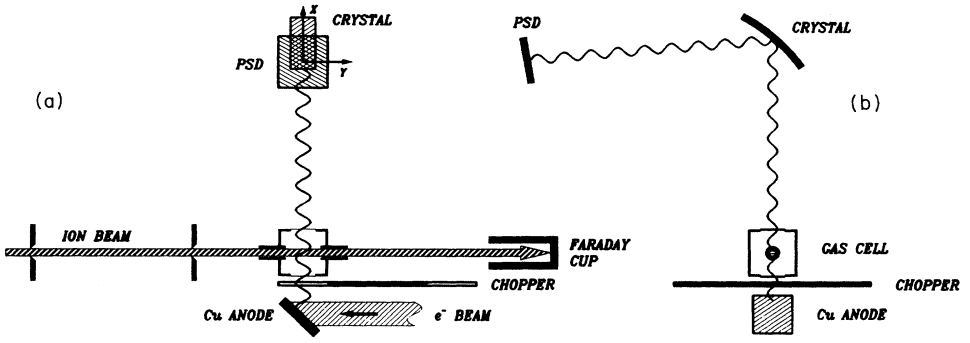

FIG. 1. Schematic of the apparatus: (a) side view, and (b) cross-sectional view.

in the x direction of about 150 μm is achieved. Simultaneously, position information perpendicular to the direction of dispersion (y direction) is gained by identifying the wire that is closest to the ionizing event. This is achieved by connecting the wires in a meandering structure and examining the charge signals at each end. The x scale of the detector was precisely calibrated for the 12 individual wires used in the experiment by means of a collimated ^{55}Fe source mounted in front of the detector on a precision linear slide.

The x-ray spectra originating from the fast ion beam are steadily compared to the Cu $K\alpha$ spectrum, which served as a wavelength standard. This is achieved by placing the Cu anode of a 15-keV x-ray generator close to the gas cell. A chopper wheel synchronized to the time structure of the UNILAC beam transmits copper x rays only during the 15-ms-long "off" periods of the pulsed ion beam. Sample spectra of both the Cu $K\alpha$ standard and of the Lyman α lines of Ni^{27+} are shown in Fig. 2. The Cu $K\alpha$ spectrum is fitted with four components of symmetric Voigt profiles on top of a linear background, and the nickel spectra are fitted with two symmetric Gaussians, also on a linear background.

As a wavelength standard, we use the Cu $K\alpha_1$ wavelength,

$$\lambda_0 = 1.540\,594\,6(23)\ \text{Å}\ , \tag{1}$$

as given by Kessler *et al.*[11] and corrected for new measurements of the interplanar spacing of silicon.[12,13]

The pattern of an x-ray image in the Johann geometry as used in the present experiment was studied in detail previously[14] for both a stationary and a fast-beam x-ray source. In Ref. 14 an analytical formula for the position of the x-ray image in the detector's x-y plane was given and was shown to agree with detailed Monte Carlo ray-tracing calculations on the 1-ppm level of wavelength accuracy.

In the data reduction of the present experiment, we will use the analytical result expressing, at a given detector height y, the separation x (in mm) between the Cu $K\alpha_1$ position and the position of one of the fast-beam Lyman α lines:

$$x = x(y;\beta,w)\ . \tag{2}$$

The analytical form of Eq. (2) is presented in the Appendix. This fit function contains, as fit parameters, the beam velocity β and an angular term w that gives the deviation of the crystal spectrometer from its perpendicular orientation relative to the ion-beam axis. In addition, geometrical constants of the apparatus are required. We also included a correction which takes into account the observed imperfections in the crystal bending.

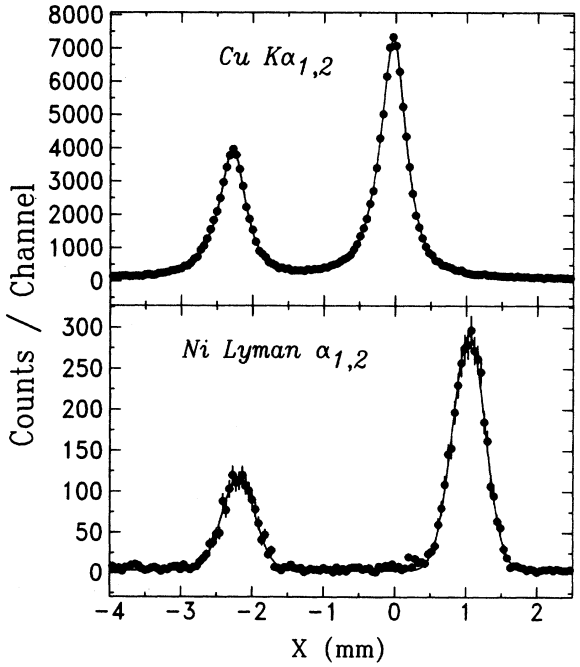

FIG. 2. Sample spectra of the Cu $K\alpha_{1,2}$ calibration standard and of the Lyman $\alpha_{1,2}$ lines of Ni^{27+} at a specific energy of 5.2 MeV/amu. The spectra are taken from an anode wire close to the center of the detector. The calibration of the abscissa, in mm, was obtained with the ^{56}Fe source, and the zero point was set to the position of the Cu $K\alpha_1$ line.

III. RESULTS AND DISCUSSION

As shown in Fig. 2, all spectra were fitted either with Voigt or Gaussian profiles in order to find the line positions. Figure 3 shows an example of the curved shape of the Cu $K\alpha_1$ line, together with a parabola fitted to the experimental data. The parabola is obtained for a stationary source if one takes the analytical form of Eq. (2), as given in the Appendix, dropping all fast-beam contributions. Inserting the geometrical constants, one obtains, for the shape of the calibration line,

$$x = x_0 - 2.87 \times 10^{-4} y^2 , \tag{3}$$

where y is given in millimeters. This is exactly the fit function used, x_0 being the only free parameter. A similar result is obtained for the Cu $K\alpha_2$ line.

The Cu $K\alpha_{1,2}$ splitting was used to check the spectrometer dispersion. From the geometrical data given in the Appendix and the copper wavelengths,[11] we calculate a splitting of $\Delta_{\mathrm{Cu,theor}} = 2261.2 \pm 3$ μm, whereas the measured value is $\Delta_{\mathrm{Cu,expt}} = 2262.2 \pm 1$ μm. The agreement is very encouraging.

Figure 4 shows the Lyman $\alpha_{1,2}$ lines of Ni^{27+} relative to the Cu $K\alpha_1$ line at the four different beam energies mentioned above. Going from low to high beam energy, the Lyman α doublet moves towards lower x (corresponding to lower x-ray energy) due to the Doppler effect at a $\sim 90°$ observation angle. Also shown in Fig. 4 is the result of a simultaneous fit to the Lyman α_1 and α_2 lines. The fit function is given by Eq. (2). Excluded from the fit are the two end wires at either side of the detector. This is done in order to ensure that end effects due to electric-field deviations do not influence the results.

From the fit, the Lyman α_1 wavelength is obtained,

$$\lambda_{\mathrm{Ni}\,\alpha_1} = 1.530\,336(20) \text{ Å} , \tag{4}$$

and the angular term is

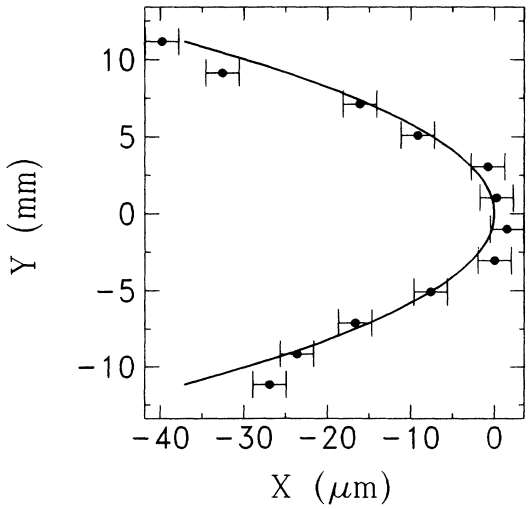

FIG. 3. The curved image of the Cu $K\alpha_1$ line due to the finite crystal height. The solid line through the data points is the predicted shape as given in Eq. (A1).

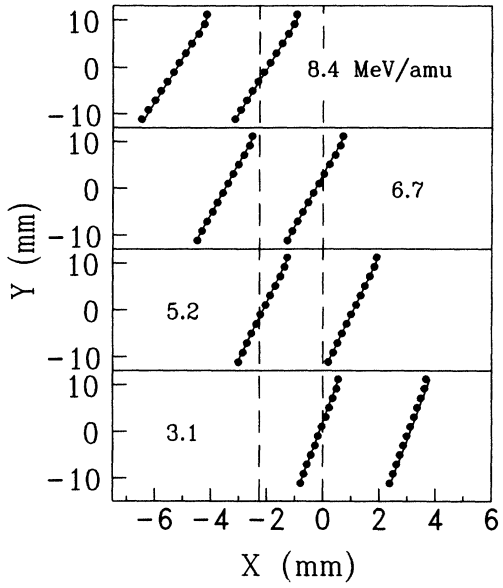

FIG. 4. The two-dimensional image of the Lyman $\alpha_{1,2}$ doublet of Ni^{27+} at four different beam energies. The solid lines represent the model of Eqs. (2)–(4). The two dashed vertical lines indicate the positions of the Cu $K\alpha_{1,2}$ lines.

$$w = 1.14 \times 10^{-3} . \tag{5}$$

This would correspond to a misalignment of the Rowland circle relative to the perpendicular orientation of about 0.07°. The data have been analyzed and the error estimated by two independent methods, both giving consistent results.

Given in Table I are the error contributions that lead to the total uncertainty in Eq. (4). The statistical errors of 5 ppm include all statistical errors of the peak-fitting procedures, in addition to the uncertainty of the detector's position response. We include a 10-ppm error, which takes into account residual uncertainties in the crystal bending. With the wavelength given in Eq. (4), the 1s Lamb shift is obtained by subtracting—from the corresponding transition energy—the calculated Coulomb energy corrected for reduced mass, and by correcting for the small QED correction[15] of the $2p_{3/2}$ state. In Table II the result is compared with the calculation of Johnson and Soff.[15] Our experimental error is

TABLE I. Error contributions (in ppm) to the wavelength uncertainty.

Error contributions	
Statistical	5
Combined crystal and detector uniformity	10
Beam velocity	3
Geometrical constants (l,$2d$, . . .)	6
Calibration line	1.5
Total	13

TABLE II. Experimental and theoretical 1*s* Lamb shift of Ni^{27+} (in eV).

Experiment[a]	Theory[b]
5.07(10)	5.096(4)

[a]Present work.
[b]Reference 15.

±2.0%. Within this error, good agreement with theory is obtained. In Fig. 5 we have plotted the difference between theory and experiment for $2l \rightarrow 1s$ transition energies, normalized to the theoretical Lamb shift. We have included all points between $Z=1$ and 36 for which a measurement is available. Experimental values are from Refs. 1–7 and theoretical ones from Ref. 15. On the same figure, we have plotted the higher-order contribution to the self-energy, normalized to the Lamb shift. Our experiment provides a new point halfway between the only two other precise points ($Z=18$ and 36). The argon value was obtained with a recoil-ion source, in which satellite contamination (due to the huge capture cross section) is difficult to keep under control. The krypton value was obtained in a beam-foil experiment with a very fast beam, a solid target, and at only one beam energy. In the latter case, the Doppler effect is difficult to control. The good agreement with theory attained in our experiment, which is not subject to the above-mentioned problems, thus strongly reinforces the confidence in the good agreement already observed for argon and krypton.

Two main points have emerged from this work: In the first instance, we have secured a new value for the 1*s* Lamb shift of H-like Ni that is believed to be more accurate than those provided by previous measurements in this region of Z. Our value is also more significant in comparison with higher-order QED effects than any of its predecessors at higher or lower values of Z, as shown in Fig. 5. Secondly, the above-mentioned result was gained in the face of conspicuous and correctable deficiencies in the experimental arrangements. For example, we have subsequently been able to prepare a crystal of the type used in this experiment, but with orientation errors which are 20 times smaller. Likewise, the detector performance has been shown to be rapidly improvable, both in resolution and linearity, over what was previously available for measurements of this type.

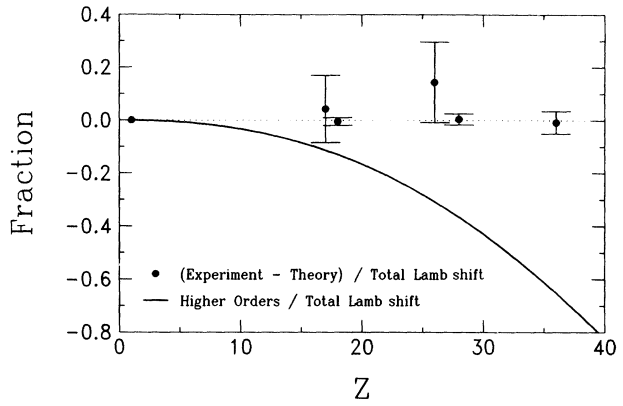

FIG. 5. Experimental minus theoretical 1*s* Lamb shift, divided by the theoretical Lamb shift as a function of the nuclear charge. The solid line represents the relative contribution of higher-order terms proportional to $(Z\alpha)^n$, $n \geq 6$.

ACKNOWLEDGMENTS

We gratefully acknowledge the skillful operation of the UNILAC by the operating staff. Without their efforts, this experiment would not have been possible. Essential improvements in the performance of the two-dimensional position-sensitive detector have been achieved by A. Henins, who also helped in bending and testing the crystal. Technical assistance before and during the experiment by W. Enders and H. Wesp is greatly appreciated.

APPENDIX: GEOMETRICAL DETAILS AND THE FIT FUNCTION

Following the analytical calculation of Ref. 14 for a Johann geometry, the separation x between the position of the calibration line and a line originating from the fast beam can be expressed as

$$x = l \tan(\arcsin H_0 - \arcsin H_1) + \Delta x + \delta x \ , \tag{A1}$$

where [cf. Eqs. (33)–(35) of Ref. 14]

$$H_0 = \lambda_0 (2d)^{-1} \{1 + [y/(l+s_0)]^2\}^{1/2} \tag{A2}$$

and

$$H_1 = \lambda_1 (2d)^{-1} (1-\beta^2)^{-1/2} (\{1 + [y/(l+s_1)]^2\}^{1/2} - \beta[(1-\epsilon)w + y/(l+s_1)]) \ . \tag{A3}$$

In Eqs. (A1)–(A2), the following constants are used: the crystal-detector separation,

$$l = 752.3 \text{ mm} \ ;$$

the crystal-source separation for the calibration source,

$$s_0 = 506 \text{ mm} \ ;$$

and, for the fast-beam source,

$$s_1 = 439 \text{ mm} \ .$$

The ion-beam velocity β is determined by the time-of-flight measurement. For the crystal's effective $2d$ value at 31 °C for second-order diffraction, also including the index-of-refraction correction, we use

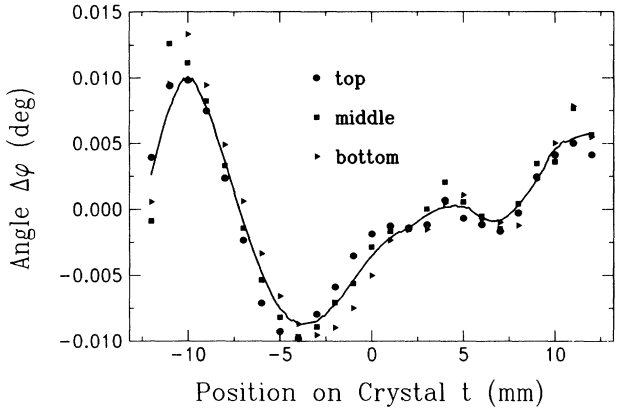

FIG. 6. Angular deviations of the crystal surface from a perfect cylinder.

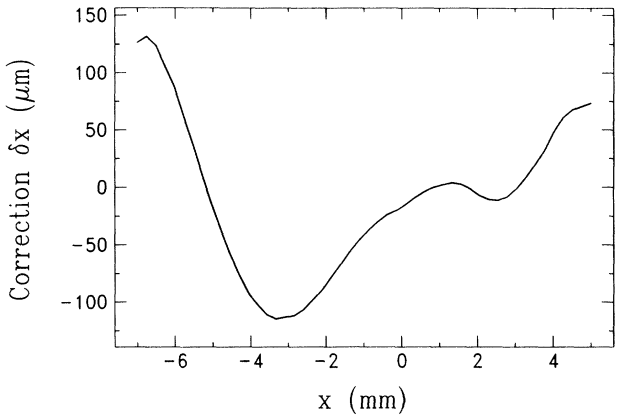

FIG. 7. Correction for crystal nonuniformity as a function of the detector coordinate.

$$2d = 2.000\,39 \text{ Å} .$$

The constant ϵ is given by

$$1-\epsilon = 2\sin(\tau_{0,\text{eff}}/2)/\tau_{0,\text{eff}} ,$$

with $\tau_{0,\text{eff}}$ denoting the effective crystal width divided by the radius of curvature of the crystal. In the present case, ϵ is

$$\epsilon = 2.6\times 10^{-6} .$$

In Eq. (A3), w denotes an angular term defining the orientation of the Rowland-circle plane relative to the ion-beam direction,

$$w = \cos\Psi \cos\varphi , \tag{A4}$$

with the angles Ψ and φ as defined in Ref. 14. We note that a displacement of the detector out of the Rowland-circle plane by an amount Δy will give another additive constant in Eq. (A3). Therefore, we interpret the parameter w to be the angular term of Eq. (A4), plus a term $-\Delta y/(l+s_1)$ due to detector misalignment.

Equation (A1) contains a small correction term Δx that is due to the combined effect of finite source heights and widths introduced by slightly different source geometries for the copper and nickel sources. For the present case, the correction is only

$$\Delta x = 0.30\pm 0.15 \ \mu\text{m} .$$

The additional correction term δx takes into account deviations of the crystal from a perfect cylinder. This quantity was measured by mapping the crystal's reflection geometry with a collimated x-ray source. Three different scans along the crystal's dispersive direction t were produced taken at a top, middle, and bottom position of the crystal height. The results are shown in Fig. 6 in terms of the local angular deviation, $\Delta\varphi$, along the crystal surface t. The solid line represents a smoothed approximation of the mean values used to construct the correction

$$\delta x(x) = l\,\Delta\varphi(t(\lambda(x))) ,$$

which is shown in Fig. 7. The correspondence between the location t on the crystal where the x ray is reflected and the detector's x coordinate is obtained by inverting the nearly linear function $t(\lambda)$, which can be expressed analytically, and taking the dispersion relation $\lambda(x)$ given in Ref. 6. The location of the $K\alpha_1$ line on the curved crystal was determined within ± 1 mm by a knife-edge shield brought close to the crystal surface.

[1]C. Wieman and T. Hänsch, Phys. Rev. A **22**, 192 (1980).
[2]M. G. Boshier, P. E. G. Baird, C. J. Foot, E. A. Hinds, M. D. Plimmer, D. N. Stacey, J. B. Swan, D. A. Tate, D. M. Warrington, and G. K. Woodgate, Phys. Rev. A **40**, 6169 (1989).
[3]J. P. Briand, M. Tavernier, P. Indelicato, R. Marrus, and H. Gould, Phys. Rev. Lett. **50**, 832 (1983).
[4]M. Tavernier, J. P. Briand, P. Indelicato, D. Liesen, and P. Richard, J. Phys. B **18**, L327 (1985).
[5]E. Källne, J. Källne, P. Richard, and M. Stöckli, J. Phys. B **17**, L115 (1984).
[6]H. F. Beyer, R. D. Deslattes, F. Folkmann, and R. E. LaVilla, J. Phys. B **18**, 207 (1985).
[7]R. D. Deslattes, R. Schuch, and E. Justiniano, Phys. Rev. A **32**, 1911 (1985).
[8]H. Geissel, Y. Laichter, R. Albrecht, T. Kitahara, J. Klabunde, P. Strehl, and P. Armbruster, Nucl. Instrum. Methods **206**, 609 (1983).
[9]G. G. Luther, P. L. Cowan, A. Henins, and S. Brennan, Nucl. Instrum. Methods A **246**, 537 (1986).
[10]P. Indelicato, A. Henins, and R. D. Deslattes (unpublished).
[11]E. G. Kessler, R. D. Deslattes, D. Girard, W. Schwitz, J. Jacobs, and O. Renner, Phys. Rev. A **26**, 2696 (1982).
[12]P. Becker, P. Seyfried, and H. Siegert, Z. Phys. B **48**, 17 (1982).
[13]R. D. Deslattes, M. Tanaka, G. L. Greene, A. Henins, and E. G. Kessler, IEEE Trans. Instrum. Meas. **IM-36**, 166 (1987).
[14]H. F. Beyer and D. Liesen, Nucl. Instrum. Methods A **272**, 895 (1988).
[15]W. R. Johnson and G. Soff, At. Data Nucl. Data Tables **33**, 405 (1985).